Waveguide for Vortex Mode Generation in HVAC Cloud Management Communication

N. Ali[1, 3, a)], A. Amphawan[2], M. Hariz Hafizalshah[1], S. A. Aljunid[3], R. Endut[3], C. B. M. Rashidi[2], M. N. M. Yasin[4], and M. I. Shapiai[5]

[1]*Semiconductor Photonics & Integrated Lightwave Systems (SPILS), School of Microelectronic Engineering, Universiti Malaysia Perlis, Pauh Putra Main Campus, 02600, Arau, Perlis, Malaysia*
[2]*Smart 5G Optical Lab, University Malaysia of Computer Science & Engineering, 3410 Jalan Teknokrat 3, Cyber 4, 63000 Cyberjaya, Selangor, Malaysia*
[3]*Advanced Communication Engineering, Centre of Excellence, Universiti Malaysia Perlis, 02600 Arau, Perlis, Malaysia.*
[4]*Bioelectromagnetics Research Group, School of Microelectronic Engineering, Universiti Malaysia Perlis, Pauh Putra Main Campus, 02600, Arau, Perlis, Malaysia*
[5]*Department of Electronic Systems Engineering, Malaysia-Japan International Institute of Technology Universiti Teknologi Malaysia, Kuala Lumpur, Malaysia*

[a)]Corresponding author: norshamsuri@unimap.edu.my

ABSTRACT. Optical modes allow for the transmission of data by propagating light in a singular coherent form along the channel. By constructing a special waveguide structure, a unique mode may be formed in a plane perpendicular to the transmission axis. This paper elucidates on the design of a waveguide to generate unique vortex modes and analyses the properties of the generated modes.

Keywords**:** Modes, vortex, mode division multiplexing, Internet-of-Things (IoT)

INTRODUCTION

In view of the capacity limits of multimode fiber in the advent of tremendous data growth, various dimensions for multiplexing and modulating data have been commercially deployed in the intensity, phase, wavelength and time dimensions. The rate at which data can be transmitted down optical fibers is approaching a limit due to nonlinear optical effects [1]. Having almost exhausted available degrees of freedom to multiplex data, the possibility of leveraging on spatial modes to enhance data capacity is now being explored [2].

Modes refer to the transverse modes of electromagnetic waves that exist in a waveguide which consist of single-mode fiber and the multi-mode fiber. The single-mode fiber only permits one mode to flow into a single channel that normally travels at a long-distance as well as consisting a large bandwidth. Its core is smaller in diameter compared to multi-mode fiber. As a contrast to single-mode fiber, multi-mode fiber permits numerous numbers of modes to pass through it that travels at a short distance and carry a small bandwidth. Various mode generation approaches have been developed in recent years, comprising spatial encryption [3-7], algorithm equalization [8-11], photonic crystal fibers [12-14] and laser cavity designs [15-16].

Optical angular momentum has garnered considerable attention for providing another degree of freedom and increasing the transmission capacity, whereby the photons are given a well-defined twist or helicity. Chen Ji et al. (2018) proposed a single-layer metasurface constructed using resonant and geometric phase cells for generating vortex beams with different OAM modes and polarizations carried at two distinctive bands [17]. Bozinovic et al. (2013) discuss the findings on the propagation of OAM modes in rectangular multimode waveguides [18]. Due to the multimode interference effect, OAM mode input forms a self-image image at certain propagation distances. As OAM modes can be decomposed as the superposition of a pair of quarter-wave phase-shifted even and odd modes, their symmetry properties lead to two different self-imaging categories – forming the OAM-maintaining

The 2nd International Conference on Applied Photonics and Electronics 2019 (InCAPE 2019)
AIP Conf. Proc. 2203, 020059-1–020059-8; https://doi.org/10.1063/1.5142151
Published by AIP Publishing. 978-0-7354-1954-4/$30.00

and the field-splitting self-images. Ma et al. (2015) utilizes the multimode interference theory to demonstrate OAM mode generation using rectangular waveguides propagating several modes with symmetry in two orthogonal transverse directions [19].

Laser light with a Laguerre-Gaussian amplitude distribution is found to form a well-defined OAM [20]. An astigmatic optical system may be used to transform a high-order Laguerre-Gaussian mode into a high-order Hermite-Gaussian mode reversibly. The experiment proposed to measure the mechanical torque induced by the transfer of OAM associated with such a transformation. Zhang et al. (2015) studied the coupling characteristics of OAM modes routing in a ring fiber based directional coupler [21]. The OAM mode propagates along a ring fiber coupler into its corresponding HE even and odd modes using beam propagation method. The general description of OAM modes in a ring fiber based coupler provides useful information for further study of fiber components using OAM modes. More recently, Tandjè et al. (2019) designed a ring-core PCF to support four different groups of OAM using a circular ring core around a cladding comprising air holes organized in a first circular ring surrounded by hexagonal rings [22]. In this paper, vortex modes are formed from the transverse refractive index variation of an optical fiber. The mode generation principles and simulations are discussed in the next section.

METHODOLOGY

Modes are uniquely formed patterns that are influenced by factors attributed to the design process. Unique modes are generated by altering the parameters of the transmitter component. These modes are modified in such a way as the phase values correspond to the particular angle around the axis. This property makes up the description of an optical vortex. The topological charge is indicated by the number of helical surfaces of the propagating wavefront. The manipulation of this factor is employed to produce a desired number of modes.

The optical vortex phase plate is a unique optic that comprised entirely of spiral or helical phase steps to control the phase of the transmitted beam. The winding "staircase" surface structure is demonstrated in Fig. 1.

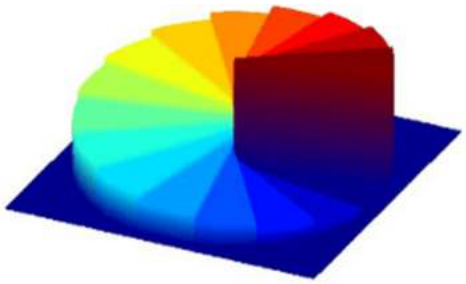

FIGURE 1. Winding "Staircase" surface profile of the diffractive vortex phase plate.

The total etching depth from the top to bottom of the "staircase" is a function of the substrate's optical index and design wavelength. Generally, this depth is of the same order of magnitude as the design wavelength. Therefore, each vortex phase plate is wavelength specific.

The topological charge, denoted in the literature as m, refers to the number of 2π cycles (i.e. "staircases") etched around 360° turn of the diffractive surface. In Fig. 2 below, the surface profiles are illustrated for vortex lenses with m=2, m=3, and m=4. The effect of a higher topological charge is an increase in the angular momentum of the vortex beam by a factor of m. An increase in the number of phase cycles within the phase profile may also be observed.

A modal coupler waveguide is designed from an optical fiber using the bmp2ind tool as seen in Fig. 3. The bmp2ind tool converts the phase gradation of a mode into the refractive index distribution of the mode.

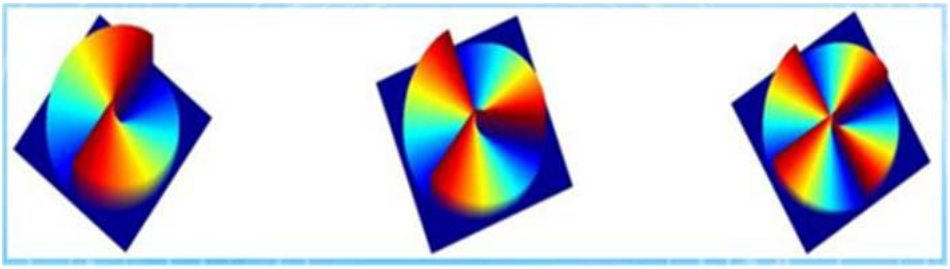

FIGURE 2. Surface profiles for Vortex lenses with m=2, m=3 and m=4.

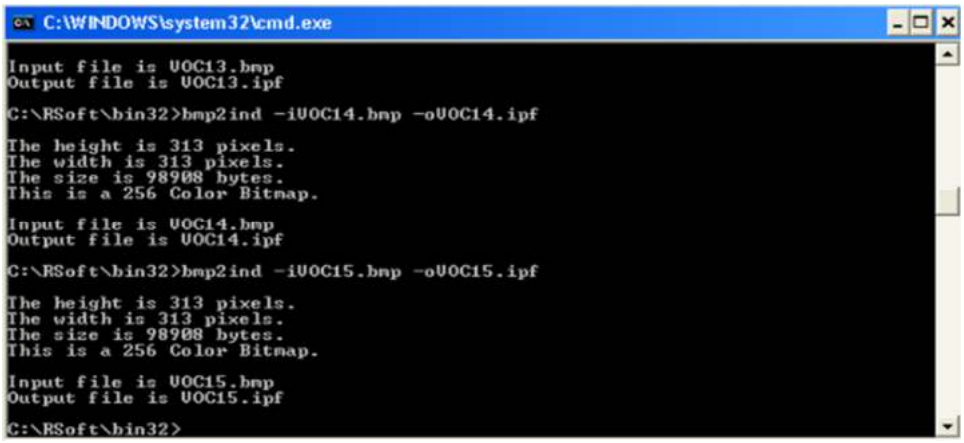

FIGURE 3. Executing the bmp2ind tool

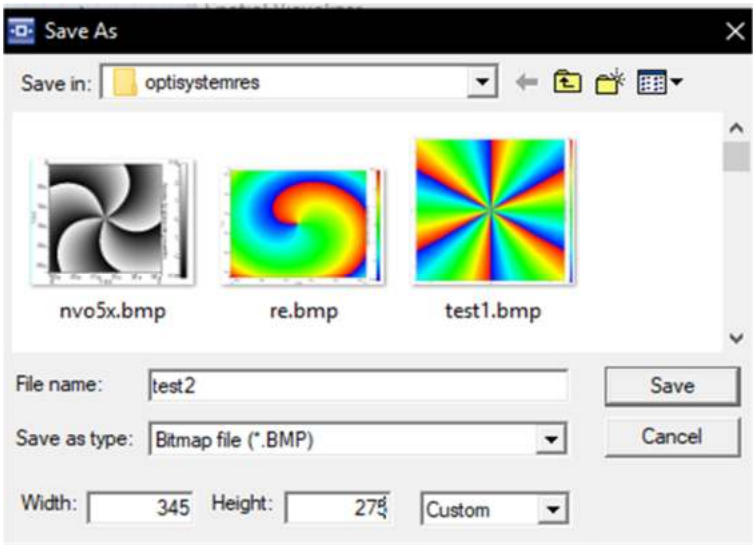

FIGURE 4. Saving the modal phase distribution as a 345 by 275-pixel image.

After obtaining the modal amplitude and phase distribution results from OptSim, the data is then saved as a .bmp file with a specific resolution value as shown in Fig. 4. Saving as a 345 by 275 pixel .bmp image produces distribution values of the mode at a 1:1 height to width ratio when cropped using an image editing tool as seen in Fig. 5.

The amplitude and phase properties of multiple modes are summed in a mathematical function and are then run through the fast Fourier transform function by MATLAB. The resulting variable produced is a complex array. The real values of the array represent the amplitude whereas the imaginary values represent the phase. The real

and imaginary values could be viewed by the abs and angle MATLAB function to view the amplitude and phase values respectively.

The angle function selects only the imaginary values of the data within the array whereas the abs function displays only the real values. The imaginary values are the component used to obtain the refractive index. The subplot function which is typically used with the imagesc function plots an arrangement of determined elements for displaying multiple values at once. The dlmwrite function exports the values within the arrays to an external text file. There are number of elements that must be specified within the dlmwrite function such as file name, data precision, data arrangements, and variable to be exported.

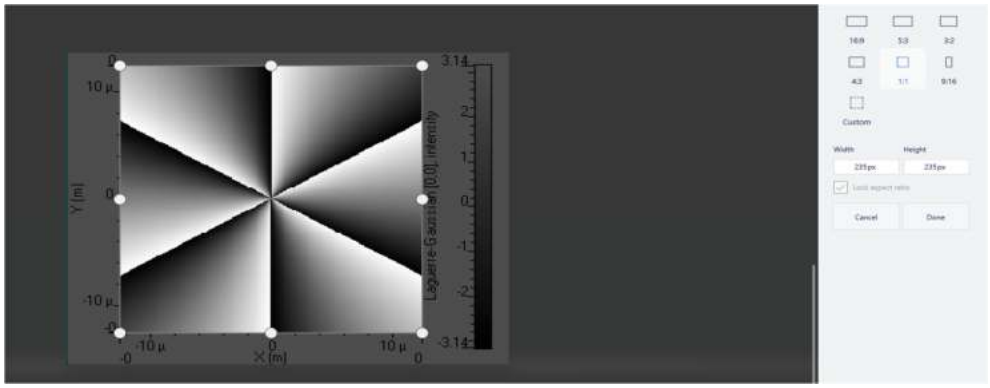

Figure 5: Cropping the results from the axes and palette.

The final step to obtaining the resulting modes from the waveguide is by the mode solver tool in BeamProp. The mode solver tool could be executed by double clicking the input plane and configuring the input wave properties and the types of data to be analyzed. The solver must be in full vector and complex mode to obtain the phase values within the modes as shown in Fig. 6.

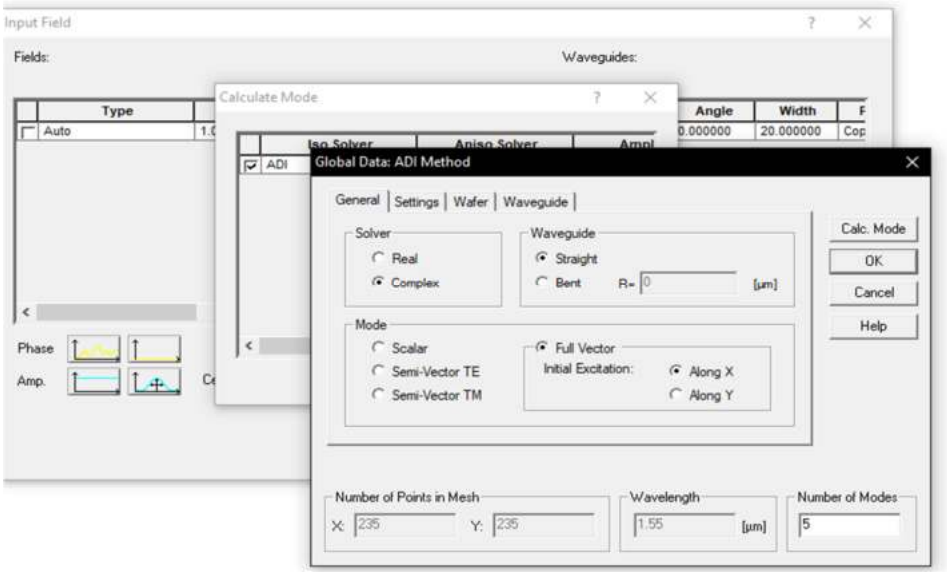

Figure 6: Solving for modes using beam propagation

RESULTS AND DISCUSSION

Running the simulation yields the amplitude and phase values, as shown in Fig. 7. The phase was cropped to a 235 by 235 pixel values of 256 bmp image format and would then be converted using the bmp2ind tool to convert it to its equivalent refractive index distribution.

The obtained refractive index distribution is then inserted into the waveguide design software BeamPROP to be simulated. The layout of the design is shown in Fig. 8. Note that the grid values are not plotted in scale to each axis value. The propagation direction is denoted by the direction of the arrow.

Alternatively, the individual vortex order modes could be multiplexed by the fast Fourier transform function via MATLAB. The individual modes are simulated using OptSim. The simulated data is then cropped and imported into MATLAB. The color of each pixel represents the values distributed. Henceforth, grayscale is greatly preferred due to the representability of the immediate color values. The data is then processed and exported into a text file which consists of the values of each cell in a specific order. The text file is then transferred to the user defined refractive index profile tool.

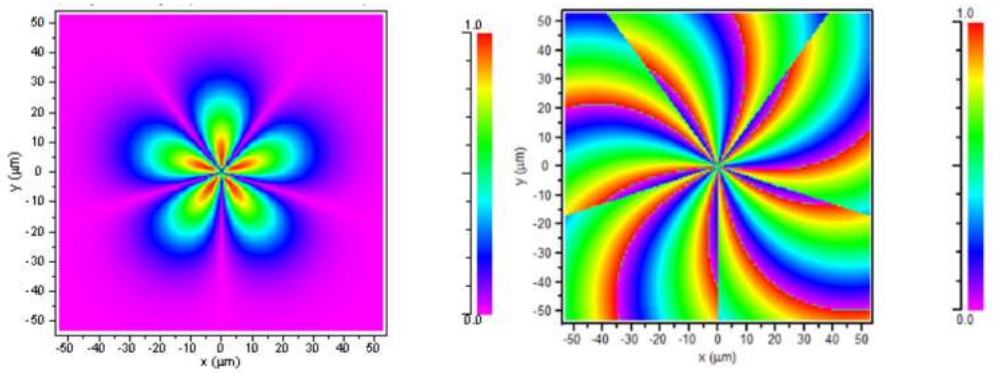

(a) (b)

FIGURE 7. (a) Amplitude and (b) phase of multiplexed vortex order 5 and 10

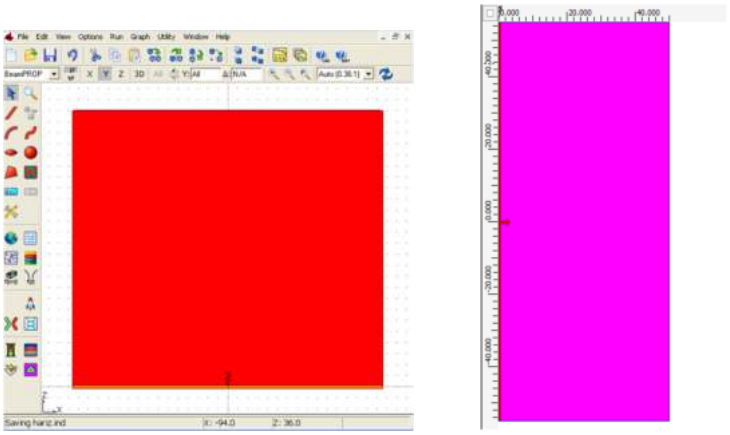

(a) (b)

FIGURE 8. (a) Waveguide design by OptSim (b) Waveguide design by BeamProp.

Topologically, the input and output planes of the waveguide are perfectly flat. The mode generation relies upon the refractive index distribution that was inserted in the waveguide as depicted in Fig. 9.

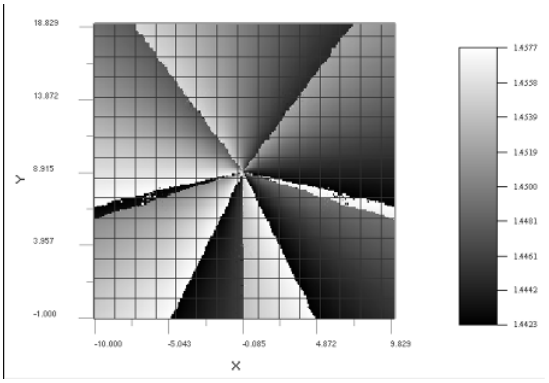

Figure 9: Refractive index distribution applied onto the waveguide.

The waveguide in Figure 8 is then simulated to obtain the mode via OptSim. The resulting mode obtained is illustrated in Figure 10. The design has been optimized by altering the propagation distance to obtain a mode most equivalent to the original mode.

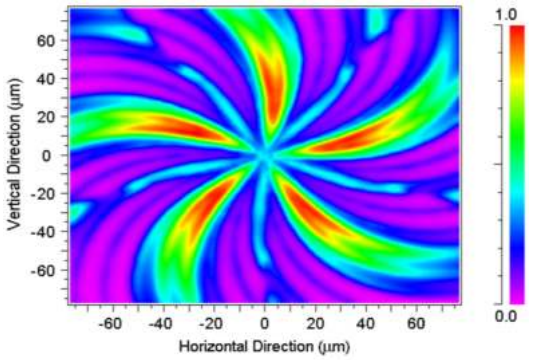

Figure 10: Modal phase of converted multiplexed phase values of vortex order 5 and 10

The waveguide performance can be measured by the eye diagram and bit error rate. This process is conducted by passing a beam of data at 9GHz across the waveguide. The wide eye opening shows satisfactory transmission.

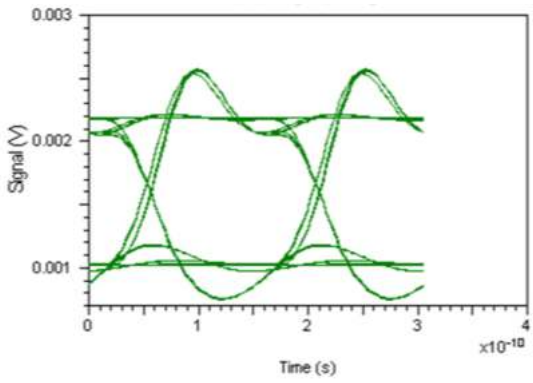

Figure 11: Eye diagram of the simulated waveguide

The bit-error-rate (BER) results are shown in Figure 12. The results of the minimum and maximum BER values are tabulated in Table 1. The BER analysis was conducted with a pseudorandom binary sequence at 9GHz. It can be deduced that the waveguide has a satisfactory data transmission rate as supported by the low BER values.

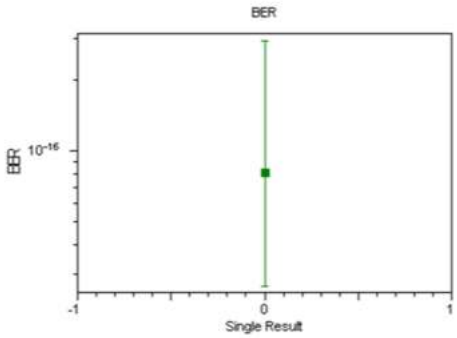

Figure 12: Bit error rate of the simulated waveguide

Table 1: BER Values from the pseudorandom source

Minimum BER	2.657 x 10 $^{-17}$
Maximum BER	2.953 x 10 $^{-16}$
Average BER	8.076 x 10 $^{-17}$

CONCLUSION

The fabrication of the waveguide requires a high degree of accuracy in the modulation of the refractive index towards achieving sufficient modal purity. The challenge is more apparent at higher vortex order values which have more intricate transverse modal distributions. Vortex mode transmission is foreseeable in realizing a sustainable optical network which may accommodate various data streams in Internet-of-Things applications.

ACKNOWLEDGMENTS

The authors acknowledge financial support by the School of Microelectronic Engineering, Universiti Malaysia Perlis (UniMAP). NA also acknowledges financial support by Universiti Malaysia Perlis STG Grant 9001-00494. The work conducted in collaboration with the Optical Technology Research Laboratory, Universiti Utara Malaysia as part of the industrial training partnership and the Fundamental Research Grant Scheme FRGS/1/2016/STG02/UUM/02/1.

REFERENCES

1. L. Allen, M. W. Beijersbergen, R. J. C. Spreeuw and J. P. Woerdman, Physical Review A **45** (11), 8185-8189 (1992).
2. A. Amphawan, Opt. Eng. **50**, 102001 (2011).
3. D. Deng, Y. Li, Y. Han, J. Ye, Y. Liu and H. Zhao, Optics Communications **428**, 84-88 (2018).
4. A. Amphawan and Y. Fazea, Optical Eng. **55** (10), 106109-106109 (2016).
5. G. Zhu, Z. Hu, X. Wu, C. Du, W. Luo, Y. Chen, X. Cai, J. Liu, J. Zhu and S. Yu, Opt. Express **26** (2), 594-604 (2018).
6. Y. Fazea and A. Amphawan, in *J. Optical Commun.* (2015), Vol. 36, pp. 327–333.
7. A. Amphawan, S. Chaudhary and B. B. Gupta, International Journal of Sensors Wireless Communications and Control **5** (1), 13-18 (2015).
8. D. Lee, K. Shibahara, T. Kobayashi, T. Mizuno, H. Takara, A. Sano, H. Kawakami, T. Nakagawa and Y. Miyamoto, J. Lightw. Technol. **34** (8), 1754-1761 (2016).

9. S. Yasear and A. Amphawan, **162**, 01023 (2017).
10. A. Noori, A. Amphawan, A. Ghazi and S. A. A. Ghazi, Bulletin of Electrical Engineering and Informatics **8** (1), 127-135 (2019).
11. Y. Fazea and A. Amphawan, in *Journal of Optical Communications* (2018), Vol. 39, pp. 175.
12. H. Zhang, W. Zhang, L. Xi, X. Tang, X. Zhang and X. Zhang, IEEE Photonics Technology Letters **28** (13), 1426-1429 (2016).
13. A. Amphawan, B. Nedniyom and N. M. Al Samman, Journal of Modern Optics **60** (20), 1675-1683 (2013).
14. T. Masunda, A. Amphawan, S. Alshwani and A. Aldawoodi, in *2018 IEEE 7th International Conference on Photonics (ICP)* (IEEE, Langkawi, 2018), Vol. 1, pp. 1-3.
15. R. Brüning, S. Ngcobo, M. Duparré and A. Forbes, Opt. Lett. **40** (3), 435-438 (2015).
16. A. Amphawan and Y. Fazea, Journal of the European Optical Society-Rapid Publications **12** (1), 12 (2016).
17. C. Ji, J. Song, C. Huang, X. Wu and X. Luo, Opt. Express **27** (1), 34-44 (2019).
18. N. Bozinovic, Y. Yue, Y. Ren, M. Tur, P. Kristensen, H. Huang, A. E. Willner and S. Ramachandran, **340** (6140), 1545-1548 (2013).
19. Z. Ma, H. Chen, K. Wu, Y. Zhang, Y. Chen and S. Yu, Opt. Express **23** (4), 5014-5026 (2015).
20. J. Dong and K. S. Chiang, IEEE Photonics Technology Letters **26** (17), 1766-1769 (2014).
21. Y. Zhang, Y. Chen, Z. Zhong, P. Xu, H. Chen and S. Yu, Optics Communications **350**, 160-164 (2015).
22. A. Tandjè, J. Yammine, M. Dossou, G. Bouwmans, K. Baudelle, A. Vianou, E. R. Andresen and L. Bigot, Opt. Lett. **44** (7), 1611-1614 (2019).